

Preparation and characterization of nanocomposites in system as: $\text{SnO}_2\text{-xTiO}_2$ (where $x = 25, 50$ and 75 mol\%)

M. A. Ahmed · El Sayed Yousef · M. F. Abdel-Messih

Received: 7 March 2011 / Accepted: 25 July 2011 / Published online: 9 August 2011
© The Author(s) 2011. This article is published with open access at Springerlink.com

Abstract Nanocomposite samples containing various molar compositions of tin and titanium oxides were synthesized by a sol–gel method using octadecylamine as controlling template agent. The structural and the crystalline features of the samples were investigated with Fourier Transformer Infra-red, X-ray diffraction, Transmission electron microscope (TEM) where the surface area was estimated by BET analysis. The crystalline parameters and the particle size were estimated by Rietveld quantitative phase analysis. It is interesting to mention that a reduction in the lattice parameters was detected upon introduction of various molar compositions of titanium oxide revealing that a part of titania is incorporated into the SnO_2 lattice forming $\text{Ti}_{1-x}\text{Sn}_x\text{O}_2$ solid solution. The quantitative analysis claims that part of titanium oxide is incorporated substitutionally in the crystal lattice of SnO_2 , forming a solid solution and other parts are either segregated as separate rutile titania phase or dispersed as amorphous phase on the grain boundary of SnO_2 . The results show a remarkable reduction in particle size from 42 to 5 nm and increasing in the specific surface area up to $176 \text{ m}^2/\text{g}$ upon introduction of various content of titania implying the role of titania particles in preventing SnO_2 crystallites from

further growing up during the progress of calcination. TEM images show that pure tin oxide particles arranged in large aggregation in wormhole like structure, while the existence of titanium oxide are successfully creates spherical nanoparticles system organized in a definite structure. The optical absorbance spectra indicate a red shift and band gap narrowing upon introduction of titania which increase with increasing in titania contents.

Keywords Composite materials · Sol–gel process · X-ray · TEM · Optical parameters

1 Introduction

Nanocomposites have paid more attention over the last decades owing to their exceptional and novel chemical and physical properties that are not exist in the bulk. The physical features of the nanoparticles including their small particle size and high surface area extends their application in many potential fields. Tin oxide is powerful semiconductor which is usually involved in gas sensors [1–3], optoelectronic devices [4, 5], dye-based solar cells [6], secondary lithium batteries electrode materials [7] and many catalytic processes [8]. Tin oxide possesses several merits as non-toxicity, low cost and high thermal stability. However, the lower surface area and poor electric resistivity are the main drawbacks that limiting its application in many catalytic and electrical fields. Many efforts have been devoted to improve the structural and electronic features of this oxide by introduction of dopants metal. More emphasize has been paid on elements of different valence. This dissimilarity in the electron redistribution can be a primary cause for creating active surface with more acidic sites. It is should be emphasized that the existence of

M. A. Ahmed · M. F. Abdel-Messih
Department of Chemistry, Faculty of Science, Ain Shams
University, Cairo, Egypt
e-mail: abdelhay71@hotmail.com

M. A. Ahmed · E. S. Yousef
Department of Physics, Faculty of Science, King Khalid
University, P.O. Box 9003, Abha, Saudi Arabia

E. S. Yousef (✉)
Department of Physics, Faculty of Science, Al-Azhar University,
Assiut Branch, Assiut, Egypt
e-mail: omn_yousef2000@yahoo.com

several dopants improve the crystalline features of SnO_2 powders through control particle size and shape [9–12]. Many authors report that the existence of iron oxide on SnO_2 surface has a dramatic role on reduction of the grain size of the samples and the resulting $\text{Sn}_{1-x}\text{Fe}_x\text{O}_2$ nanocomposite exhibit higher catalytic activity and sensor signal than both pure SnO_2 and Fe_2O_3 [9, 13]. Azam et al. [14] indicate formation of solid solution between nickel and tin oxide through incorporation of nickel in the crystal structure of tin oxide upon addition of small composition of nickel. In a newly published paper, a nanocomposites of $\text{SnO}_2\text{--Al}_2\text{O}_3$ contain various proportion of alumina were prepared by sol–gel method. Indeed, a remarkable reduction in grain size is detected upon addition of alumina which is accompanied by large increase in surface area of composites [15]. However, there is a lack in the literature on investigation the structural and textural features of $\text{SnO}_2\text{--TiO}_2$ nanocomposites. Titanium oxide has evolved as an important material in pigments [16], adhesions, catalytic supports [17], solar cell and photocatalysts [18, 19]. It is interesting to mention that both tin and titanium dioxide are *n*-type semiconductors showing several similarities in crystal structural and electronic properties. However, they differ in band energy gap value, thermal stability and surface area. The formation of nano mixed oxides may provide a new material which can possess many desirable properties which is not exist in the pure oxide as increase in thermal stability, surface area, limit the degradation in the textural properties and improve the photocatalytic activity of the samples. Recently, several authors indicate that doping of titanium oxide with appropriate composition of tin oxide improve the photocatalytic efficiency of titanium oxide by decrease the recombination of positive hole and electron which is the main drawback exist in the electronic structure of titania. Sayilkan indicates that the photoelectric conversion efficiency of the SnO_2 cell modified by colloid TiO_2 is higher than that of the TiO_2 cell without modification [20]. The photocatalytic degradation of rhodamine dye which is primary constituent of water pollution result from textile industry is enhanced for titanium oxide embedded appropriate composition of tin oxide [21]. The photocatalytic oxidation of phenol is studied by Liqiang et al. [22] using a composite of $\text{TiO}_2/\text{SnO}_2$ prepared by sol–gel method and the results revealed that a maximum catalytic activity is detected for sample exhibit 3% SnO_2 and calcined at 600 °C. In a newly published paper, Tu et al. [23] indicate that doping titanium oxide with appropriate composition of tin oxide improve the photocatalytic activity of the sample for degradation of methylene blue dye. Moreover, many recent studies reveal that $\text{TiO}_2\text{--SnO}_2$ system has various desirable electrical and optical applications compared with either pure oxide [24, 25].

Several methods have been employed to synthesis nanomaterials with definite particle size and structure such as sol–gel [26, 27], co-precipitation [28], and chemical vapor deposition [29]. The sol–gel method is the most effective and simple method in designing oxide framework with highly ordered structure. This method involves two stages which are hydrolysis of metal precursors and polycondensation of sol particles, followed by formation of metal hydroxide or oxides depending on the operating conditions [30]. The critical point in synthesis $\text{SnO}_2\text{--TiO}_2$ nanocomposite is to achieve high degree of homogeneity by controlling the hydrolysis and condensation rate during the stage of synthesis. The existence of surfactants or amphiphilic block copolymers during the progress of sol–gel stages is one of the most efficient ways not only in controlling the hydrolysis of metal salts and preventing the particles agglomeration, but also in tailoring nanocomposites of definite shape. Octadecyl amine with long hydrocarbon chain embedded in its structure is an effective surfactant which involved to control the pore structure and particle size of different composite materials [31, 32].

The motivation of this work is to synthesis $\text{TiO}_2\text{--SnO}_2$ nanocomposites by sol–gel method using octadecylamine as controlling template surfactant in attempts to control the particle shape and size. Moreover, the role of the existence of different molar composition of titanium oxide on the structure, particle size, crystalline phases, surface area and morphology of the tin oxide will be investigated. Moreover, the optical properties of the samples in particular, the absorbance spectra, band gap energy and refractive index were studied.

2 Experimental

Nanocomposites containing various molar compositions of tin and titanium oxides were synthesized by sol–gel method using octadecylamine as a template agent. An appropriate amount of $\text{SnCl}_4 \cdot 5\text{H}_2\text{O}$ (Prolabo, 99.9%) and TiCl_4 (Prolabo, 99.9%) dissolved in a mixture of ethanol and water in ratio 1:1 were mixed together with constant stirring for 2 h by certain proportion in order to obtain 0, 25, 50 and 75 mol% ratio of TiO_2 . Then, 1 g of octadecylamine (Aldrich, 99%) was dissolved in appropriate volume of ethanol just at a level at which micelle is formed, then added to the metal salt solution followed by continuous stirring. Ammonia solution (1 M) was added drop by drop to the above solution until a turbid sol is formed. The sol mixture was left for 48 h for aging in the air until the gel particles was formed. The gel particles were washing several times with de-ionized water and ethanol until all chloride ions are removed (by examining the filtrate solution using silver nitrate solution). The gel was then dried in

an oven at 80 °C for 24 h to remove moisture and physical adsorbed species, then, the dried solids were ground in an agate mortar until a fine and homogeneous powder mixture was obtained. Finally, the solids were annealed in air at 600 °C for 4 h, using a heating rate of 5 °C/min.

2.1 Material characterization

Fine and homogeneous powders of the different samples were back-loaded into the sample holder of a P Analytical X'PERT MPD diffractometer using Cu (K α 1/K α 2) radiation. The XRD patterns were recorded in a diffraction angle range from 20° to 100° with a step of 0.03° and integration time of 4 s per step. The diffraction patterns have been treated with the Rietveld refinement method using the MAUD program. The instrumental imperfections were evaluated with a sample of LaB6 calibrated against a sample of NIST SRM-640b and provided by the Gem Dugout Company.

Fourier-transform infrared (FTIR) spectra were measured at room temperature on an ATT Mattson series FTIR TM spectrometer using the KBr disk technique. The measurements were conducted in an absorbance mode within the frequency range of 4,000–400 cm⁻¹, with a resolution of 2 cm⁻¹.

Adsorption–desorption isotherms of purified N₂ at 77 K were determined using a conventional volumetric apparatus connected to a vacuum system that allowed prior outgassing to a residual pressure of 10⁻⁵ Torr.

The evolution of the morphology of the nanocomposites powders was examined by scanning microscopy (SEM) FE-SEM JEOL 6340.

The evolution of the morphology and particle size of the nano mixed oxide powders was examined by transmission electron microscopy TEM using a JEOL 2000FX microscope.

2.2 Radial distribution function (RDF) formulation analysis

The total structure factor of material of a material is given as;

$$S(k) = \frac{\{I(k) - [\langle f^2 \rangle - \langle f \rangle^2]\}}{\langle f \rangle^2}, \quad (1)$$

where $I(k)$ is being the scattered corrected X-ray intensity of the atomic species constituting the given specimen, f , is atomic scattering. $k = \frac{4\pi \sin \theta}{\lambda}$ is the magnitude of the scattering vector. The term $[\langle f^2 \rangle - \langle f \rangle^2]$ is known as Laue diffraction. This Laue term is of more significance as small angle (2θ) of scattering. The observed $S(k)$ is related

to the deviation from the average number density ρ_0 by a sine transform as [33];

$$S(k) = \frac{4\pi}{k} \int_0^\infty r[\rho(r) - \rho_0] \sin(kr) dr \quad (2)$$

where $\rho(r)$ is the atomic density as function of the radial distance, r . Here

$$\rho_0 = \frac{\rho N}{A} \times 10^{24} \quad (3)$$

where ρ is the sample density in gm/cm³, N is the Avogadro's number, A is being the sample atomic weight. RDF is given as;

$$4\pi r^2 \rho(r) = rG(r) + 4\pi r^2 \rho_0 \quad (4)$$

where $G(r)$ is the reduced RDF so;

$$G(r) = 4\pi r[\rho(r) - \rho_0] = \frac{2}{\pi} \int_0^\infty k[S(k) - 1] e^{-\alpha^2 k^2} \sin(kr) dk \quad (5)$$

$4\pi r^2 \rho_0$ is of asymptotic form and α^2 is the disordering parameter of value $\approx 0.01 \text{ \AA}^2$ mainly used to reduce the effect of spurious details in the high K -range in the measured data.

3 Results and discussion

3.1 X-ray diffraction

Figure 1a–e displays the XRD patterns of SnO₂–TiO₂ nanocomposites. The diffraction pattern of the pure SnO₂ show definite crystalline peaks at $2\theta = 26.6, 34.2, 37.6, 51.8, 54.8, 58.4, 61.9$ and 65.2° owing to the cassiterite tetragonal (rutile type) structure of SnO₂ (ICDD card No. 41-1445) of space group P4₂/mmn. However, the diffraction pattern of pure titanium oxide illustrate several peaks reflect the existence of titania rutile phase (see Fig. 1a). The diffraction pattern of the composite samples show several characteristics peaks for SnO₂ shifted to higher 2θ values in addition to three small peaks at $2\theta = 39.1, 62.1$ and 64.1 assigned to titania rutile phase. Table 1 gives the refined structural parameters obtained from Rietveld analysis. Applying the MAUD program [34], Rietveld analysis indicates a reduction in the value of lattice parameters (a , c) of tin oxide rutile phase in the composite samples, this is more pronounced in Fig. 2 where one can notice a remarkable reduction in the lattice parameters upon increasing in the molar composition of titania. Figure 3 depicts the pattern fitting resulting from Rietveld quantitative phase analysis

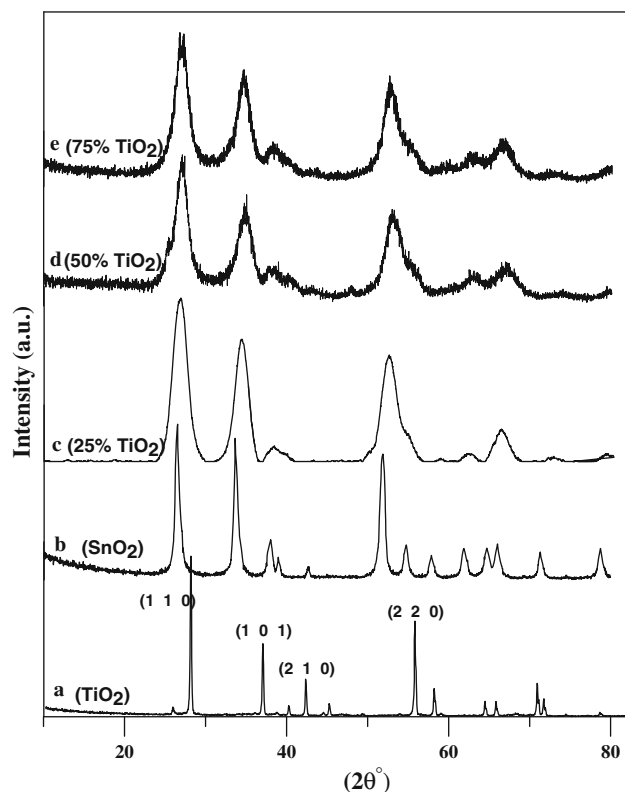


Fig. 1 X-ray diffraction of SnO_2 - TiO_2 mixed oxides, **a** TiO_2 , **b** SnO_2 , **c** SnO_2 -25% TiO_2 **d** SnO_2 -50% TiO_2 and **e** SnO_2 -75% TiO_2

Table 1 The refined lattice parameters (a and c) (Å), crystallite size D nm, obtained from Rietveld analysis of the powder XRD patterns of SnO_2 - $x\text{TiO}_2$ ($x = 0, 25, 50, 75$ mol%) compounds

X mol%	0	25	50	75
d (nm)	41	18	9	5
a (Å)	4.73789	4.6981	4.6787	4.6579
c (Å)	3.18843	3.1423	3.1166	3.0823
S_{BET} (m^2/g)	86.5	124	138	174

S_{BET} is the specific surface area (m^2/g)

for the sample containing equimolar ratio of tin and titanium oxides in which all the crystalline phases are identified, the pattern reflects the existence of rutile tin oxide as a major phase in the sample, however, the rutile titanium oxide present as a minor phase. These crystalline features imply the formation of $\text{Ti}_{1-x}\text{Sn}_x\text{O}_2$ solid solution in which Ti^{4+} ions are incorporated substitutionally in the SnO_2 lattice replacing the Sn^{4+} ions in the crystal lattice. With respect to the structural properties and ionic size of both cations, SnO_2 and TiO_2 exhibit rutile crystalline structure of space group $\text{P4}_2/\text{mmn}$ and both cations possess nearly the same ionic radius which can explaining the formation of $\text{Ti}_{1-x}\text{Sn}_x\text{O}_2$ solid solution [33–36]. The quantitative phase analysis confirms that a large part of the Ti^{4+} ions are incorporated in

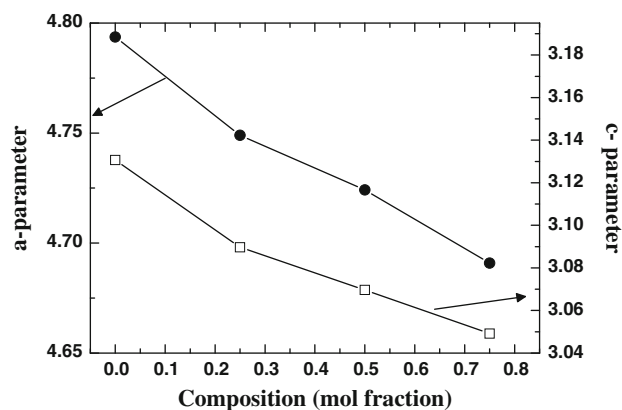


Fig. 2 Variation of the lattice parameters, a , and, c , of tetragonal SnO_2 with the mole ratio x in the composite SnO_2 - x TiO_2 (where $x = 0.0, 25, 50$ and 75%)

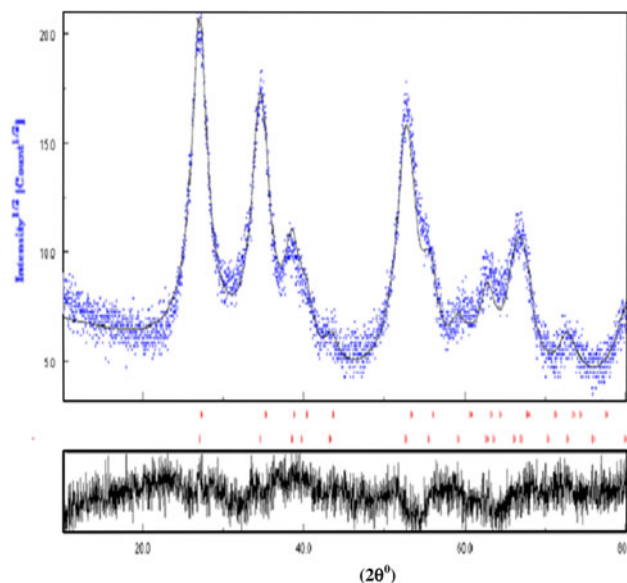


Fig. 3 The XRD profile fitting resulting from Rietveld analysis of SnO_2 - $x\text{TiO}_2$ ($x = 50$ mol %) showing the two phases

the SnO_2 lattice forming a $\text{Ti}_{1-x}\text{Sn}_x\text{O}_2$ solid solution, while part of the remainder content of titanium oxide exists as a separate rutile phase and the last part dispersed as amorphous phase between tin oxide crystallites.

On examining Fig. 1, one can notice a broadening in the peaks width which are associated with increasing in titanium oxide content indicating a strong reduction in the crystallite size of the composite samples. The particle size estimated from Rietveld analysis lie in nano scale between 46 and 6 nm depending on the titania content. The remarkable reduction in crystalline size of the samples suggests the existence of amorphous titania on the grain surface of tin oxide inhibits the crystal growth during the progress of annealing.

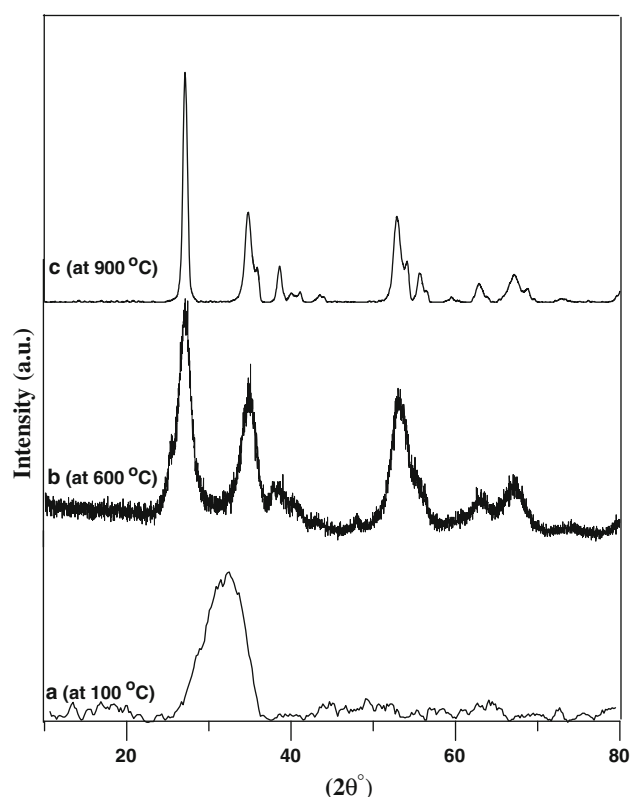


Fig. 4 X-ray diffraction of SnO_2 -50% TiO_2 annealed at different temperatures **a** tempered at 100 °C, **b** tempered at 600 °C and **c** tempered at 900 °C

More emphasize has been paid on the sample possesses equimolar ratio of the two oxides to explore the influence of annealing temperature on the crystallite size. It is interesting to notice a pronounced narrowing in the diffraction peaks upon increasing in annealing temperature (Fig. 4). This result implies that the crystallite size is more sensitive toward the annealing temperatures. A remarkable increase in the crystallite size is detected upon increasing in the annealed temperature which owing to possibility of particles agglomeration.

3.2 Surface characterization

The specific surface areas (A_{BET}) of the samples estimated by using the BET equation in its normal range of applicability and adopting a value of 16.2 Å for the cross-sectional area of N_2 are given in Table 1. The results reveal a pronounced increase in the surface area values upon increase in titanium oxide content which confirm the role of titania in preventing the small particles from agglomeration and prevent formation of large particles. This result is constituent with data obtained from X-ray measurements in which large reduction in grain size is detected for sample embedded high titania content.

3.3 FTIR measurements

Figure 5 displays the FTIR spectrum of the composites system SnO_2 -x TiO_2 . The spectrum illustrates two broad bands centered at 1,620 and 3,440 cm^{-1} which attributed to the bending and the stretching vibrations of -OH groups and physical adsorbed water, respectively [37]. It is should be interesting to mention that the hydroxyl peaks become more pronounced for samples embedded large content of titanium oxide. The two bands near 550 and 620 cm^{-1} agree with the stretching vibrations of Sn-O and Ti-O bonds [38].

Moreover, the spectrum show a small band centered at 2,300 cm^{-1} which assigned to stretched mode of vibration of CO_2 .

Several authors attribute the band centered at 620 to Sn-O bond, while a band at 550 cm^{-1} due to terminal Sn-O. On examining Fig. 5, we notice that the band centered at 620 cm^{-1} become broader as the titania content increase. However, the band centered at 550 cm^{-1} disappears completely on increase titania content. This result implies the formation of Ti-O-Sn bond as a result of homogeneous mixture of the two oxides. It is interesting to notice that as Ti content increases, the relative intensity of the peak at 621 cm^{-1} becomes stronger than that at 556 cm^{-1} , eventually disappear, a phenomenon that may relate to the

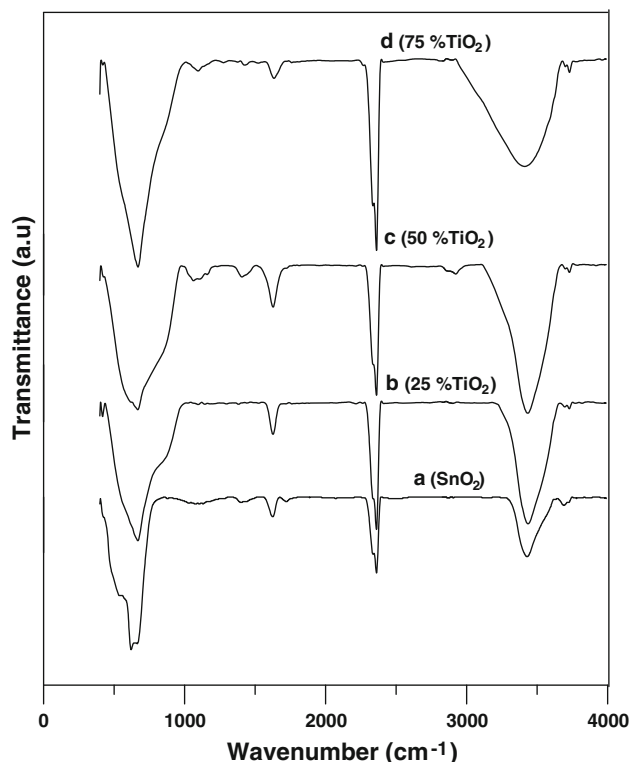


Fig. 5 FTIR of SnO_2 - TiO_2 mixed oxides system, **a** SnO_2 , **b** SnO_2 -25% TiO_2 , **c** SnO_2 -50% TiO_2 and **d** SnO_2 -75% TiO_2

crystalline state of SnO_2 nanoparticles. Zhang et al. [39] have reported that the band formed at 550 cm^{-1} in a mixture of tin and aluminum oxide is attributed to large crystallites of tin oxide, while the band centered at 620 cm^{-1} is attributed to nanoparticles. By the same manner, we conclude that disappearance of the band centered at 550 cm^{-1} reveals the role of titania on reducing the particle size of tin oxide.

3.4 Transmission electron microscope

Figure 6 depicts the TEM images of pure and mixed tin oxide samples. TEM studies provide further insight on the nanostructure of the composite sample. It is clear from the image that pure tin oxide particles exist as large aggregates in wormhole like structure. However, the composite samples contain a large number of small spherical particles arranged in definite structure. The average particle size estimated varies in range 32–8 nm depending on titania content embedded in the composite samples. TEM image

reflects that the grain size of the composite powders decrease upon increasing the titania content. The results obtained from SEM and TEM analysis are in constituent with X-ray and BET analysis.

3.5 Calculation of optical energy gap and refractive index

Mott and Davis [40] related data to the optical band gap, E_{opt} , through the following general relation proposed for materials;

$$\alpha(\nu) = \frac{B(h\nu - E_{\text{opt}})^r}{h\nu} \quad (6)$$

where $\alpha(\nu)$ is the optical absorption coefficient, the index, r , take different values depending on the mechanism of inter band transition, B is a constant and, $h\nu$, is the photon energy of incident photon. The Eq. 6, depicts a straight line for $r = 1/2$ and is associated with direct allowed transitions in crystalline material. Figure 7, represents the plot $(\alpha h\nu)^2$

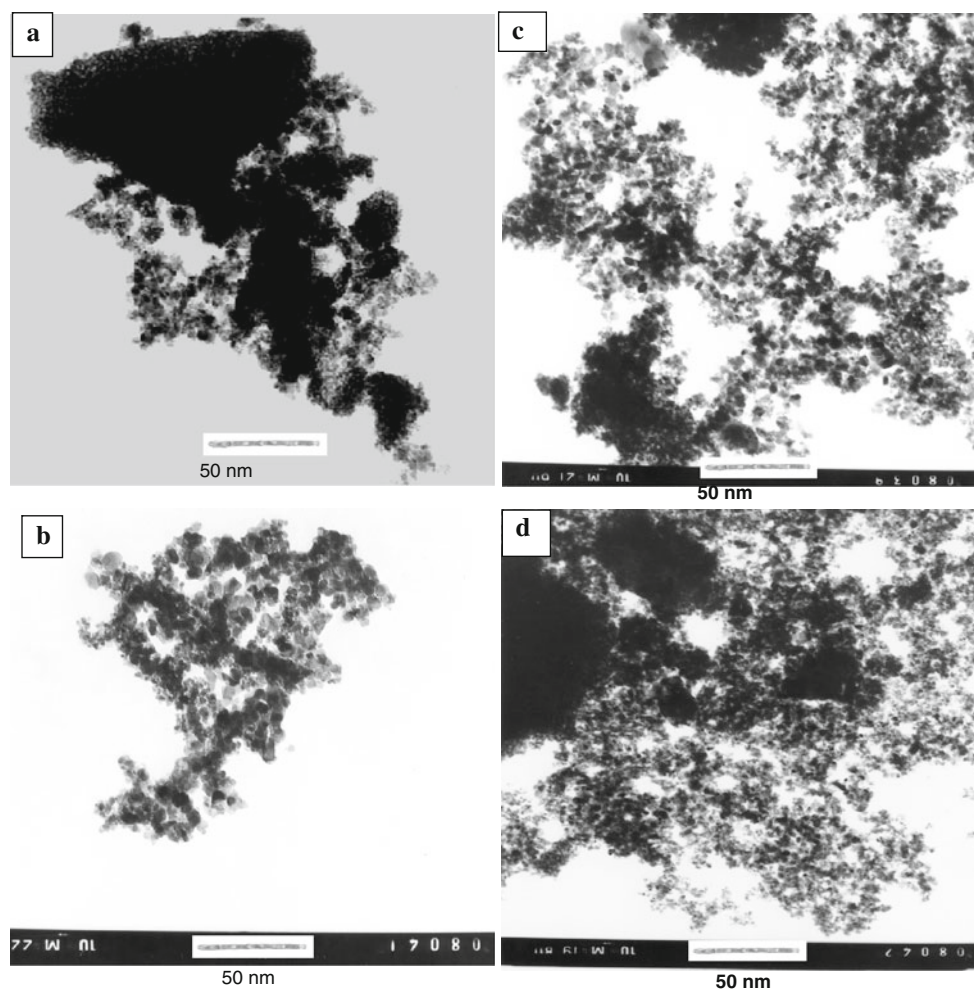


Fig. 6 TEM images of SnO_2 - TiO_2 mixed oxides system, **a** TiO_2 , **b** SnO_2 -25% TiO_2 , **c** SnO_2 -50% TiO_2 and **d** SnO_2 -75% TiO_2

versus $(h\nu)$ for the prepared samples. The E_{opt} has been estimated from the linear regions of the curves by extrapolating them to meet the, $h\nu$, axis at $(\alpha h\nu)^2 = 0$ and the The value of the optical energy gap for prepared nanocomposites samples SnO_2 -25% TiO_2 , SnO_2 -50% TiO_2 and SnO_2 -75% TiO_2 equal 3.2, 3.3 and 3.405 eV, respectively. Optical absorptions for prepared samples arise through electron transfers from the valence band to the conduction band when increasing TiO_2 wt%.

Optical electronegativity is one of the most important parameters in understanding the nature of chemical bonding. The correlation between energy gap E_g and optical electronegativity, χ , has been calculated by relation reads as follows:

$$\chi = 0.2688 E_g \quad (7)$$

The value of, χ , of prepared nanocomposites samples SnO_2 -25% TiO_2 , SnO_2 -50% TiO_2 and SnO_2 -75% TiO_2 equal 0.8602, 0.88704 and 0.9154, respectively.

The refractive index, n , is one of the fundamental properties of materials because it is closely related to average electronic oxide polarizability of ions and local field inside the material. It is can be calculated from the relation as follow [41]

$$\chi = 9.8 e^{-n} \quad (8)$$

the value of refractive index of for prepared nanocomposites samples SnO_2 -25% TiO_2 , SnO_2 -50% TiO_2 and SnO_2 -75% TiO_2 equal 2.4338, 2.4023 and 2.0315, respectively. Finally if the optical electronegativity is high the materials are considered ionic in nature and if its magnitude is less the materials are considered to be covalent in

nature. It is noticed that for molecules whose optical electronegativity value is less, their refractive index, n , and electronic polarizability are high, this valid in the present prepared SnO_2 - TiO_2 mixed oxides.

4 Conclusions

Various molar compositions of SnO_2 - TiO_2 nano composites were successfully prepared by sol-gel method using octadecyl amine as controlling template surfactant. The synthesized samples are in nanometric dimension which confirm the role of octadecyl amine in fabricating nanocomposites by preventing the agglomeration of the oxide particles. Titanium oxide particles are dispersed by several ways in the composite structure, part is incorporated into SnO_2 lattice forming $\text{Ti}_{1-x}\text{Sn}_x\text{O}_2$ solid solution and the remainder part is either segregated forming a separate rutile phase or deposited as amorphous phase on tin oxide grain surface. Increase in titania content is accompanied by large reduction in particle size and increase in the surface area of sample which reflect the role of titania in preventing tin oxide particle in growing in size. The energy gap (E_g) of the composite samples can be tuned by controlling the molar compositions of both tin and titanium oxides.

Open Access This article is distributed under the terms of the Creative Commons Attribution Noncommercial License which permits any noncommercial use, distribution, and reproduction in any medium, provided the original author(s) and source are credited.

References

1. Firooz A, Hyodo T, Mahjoub A, Khodadadi A, Shimizu Y (2010) *Sens Actuators* 147:554–560
2. Han X, Zhang B, Guan S, Liu J, Zhang X, Chen R (2008) *J Alloys Compd* 461:L26–L28
3. Wen Z, Liu T (2010) *Phys B Condens Matter* 405:1345–1348
4. Babar AR, Shinde SS, Moholkar AV, Rajpure KY (2010) *J Alloys Compd* 505:743–749
5. Hayakawa T, Nogami M (2005) *Sci Technol Adv Mater* 6:66
6. Sharma R, Mane RS, Min SK, Han SH (2009) *J Alloys Compd* 479:840–843
7. Nacimientto F, Alcántara R, Tirado JL (2009) *J Alloys Compd* 485:385–390
8. Khder AS, Ahmed AI (2009) *Appl Catal A* 354:153–160
9. Fang L, Zu X, Liu C, Li Z, Peleckis G, Zhu S, Liu H, Wang L (2010) *J Alloys Compd* 491:679–683
10. Heiba ZK, Ahmed MA, Ahmed SI (2010) *J Alloys Compd* 507:253–256
11. Wang C, Li J, Zhang Y, Wei Y, Liu J (2010) *J Alloys Compd* 493:64–69
12. Hai S, Yan C, Yu H, Xiao G, Wang D (2009) *J Alloys Compd* 488:370–373
13. Rumyantseva MN, Kovalenko VV, Gaskov AM, Pagnier T, Machon D, Arbiol J, Morante JR (2005) *Sens Actuators B* 109:64
14. Azam A, Ahmed AS, Ansari MS, Shafeeq MM, Naqvi AH (2010) *J Alloys Compd* 506:237–242

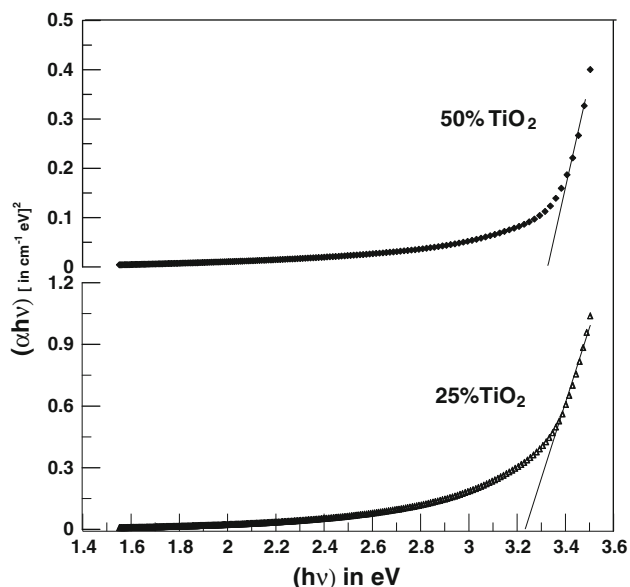


Fig. 7 $(\alpha h\nu)^2$ vs. $(h\nu)$ for the prepared samples (as example 25% TiO_2 and 50% TiO_2)

15. Heiba ZK, Ahmed MA, Ahmed SI (2010) *J Alloys Compd* 507:253–256
16. Kato S, Hirano Y, Iwata M, Sano T, Takeuchi K, Matsuzawa S (2005) *Appl Catal B* 57:109–115
17. Azizi Y, Pitchon V, Petit C (2010) *Appl Catal A* 385:170–177
18. Zheng L, Xu M, Xu T (2000) *Sens Actuators B* 66:28–30
19. Shen Y, Tao J, Gu F, Huang L, Bao J, Zhang J, Dai N (2009) *J Alloys Compd* 474:326–329
20. Sayilkan H (2007) *Appl Catal A* 319:230–236
21. Zheng SK, Wang TM, Hao WC, Shen R (2002) *Vacuum* 65:155–159
22. Liqiang J, Honggang F, Baiqi W, Dejun W (2006) *Appl Catal B* 62:282–291
23. Tu Y, Huang S, Sang J, Zou X (2009) *J Alloys Compd* 482:382–387
24. Martinez AI, Acosta DR, Cedillo G (2005) *Thin Solid Film* 490:118–123
25. Stambolova I, Blaskov V, Vassilev S, Shipochka M, Dushkin C (2010) *J Alloys Compd* 489:257–261
26. Gu F, Wang SF, Lu MK, Qi YX, Zhou GJ, Xu D, Yuan DR (2003) *Inorg Chem Commun* 6:882
27. Kurihara LA, Fujiwara ST, Alfaya RVS, Gushikem Y, Alfaya AS, de Castro SC (2004) *J Colloids Interface Sci* 274:579
28. Rumyantseva MN, Kovalenko VV, Gaskov AM, Pagnier T, Machon D, Arbiol J, Morante JR (2005) *Sens Actuators B* 109:64
29. Wang JX, Chen HY, Gao Y, Liu DF, Song L, Zhang ZX, Zhao XW, Dou XY, Luo SD, Zhou WY, Wang G, Xie SS (2005) *J Cryst Growth* 284:73
30. Chandra Bose A, Thangadurai P, Ramasamy S (2006) *Mater Chem Phys* 95:72
31. Yan X, He J, Evans DG, Duan X, Zhu Y (2005) *Appl Catal B* 55:243–252
32. Oki AR, Xu Q, Shpeizer B, Clearfield A, Qiu X, Kirumakki S, Tichy S (2007) *Catal Commun* 8:950–956
33. Liu SW, Li Y, Xie M, Guo X, Ji W, Ding W (2010) *Mater Lett* 64:402–404
34. L Lutterotti (2006) Maud 2.044, <http://www.mg.unitn.it/~Luttero/maud>
35. Carotta MC, Gherardi S, Malagù C, Nagliati M, Vendemiati B, Martinelli G, Sacerdoti M, Lesci IG (2007) *Thin Solid Films* 515:8339
36. Yu HC, Shen P (2008) *J Eur Ceram Soc* 28:91–99
37. Sbu CP, Kumar SR, Mukundan P, Warriar KGK (2002) *Chem Mater* 14:2876
38. Zhu JJ, Zhu JM, Liao XH, Fang JL, Zhou MG, Chen HY (2002) *Mater Lett* 53:12
39. Zhang J, Gao L (2004) *J Solid State Chem* 177:1425
40. Mott NF, Davis EA (1970) *Phil Mag* 22:903
41. Xinyu Z, Xiaoli W, Hai L, Zhiqiang W (2008) *Physica B* 403:2450